LETTERS

High-power GaSb-based microstripe broad-area lasers

Applied Physics Express **11**, 032702 (2018)
https://doi.org/**10.7567/APEX.11.032702**

High-power GaSb-based microstripe broad-area lasers

Zefeng Lu[1,2], Lijie Wang[1], Yu Zhang[2,3], Shili Shu[1], Sicong Tian[1], Cunzhu Tong[1*], Guanyu Hou[1,2], Xiaoli Chai[2,3], Yingqiang Xu[2,3], Haiqiao Ni[2,3], Zhichuan Niu[2,3], and Lijun Wang[1]

[1]*State Key Laboratory of Luminescence and Application, Changchun Institute of Optics, Fine Mechanics and Physics, Chinese Academy of Sciences, Changchun 130033, China*
[2]*College of Materials Science and Opto-Electronic Technology, University of Chinese Academy of Sciences, Beijing 100049, China*
[3]*State Key Laboratory for Superlattices and Microstructures, Institute of Semiconductors, Chinese Academy of Sciences, Beijing 100083, China*

*E-mail: tongcz@ciomp.ac.cn

Received November 23, 2017; accepted February 6, 2018; published online February 22, 2018

A simple and effective approach based on the microstripe broad-area (MSBA) structure was proposed, and high-efficiency and high-power mid-infrared GaSb-based quantum well lasers were demonstrated. It was shown that the MSBA structure can effectively suppress the lateral current leakage and improve the temperature behavior of GaSb lasers. Compared with the conventional broad-area structure, the energy conversion efficiency of MSBA lasers was more than threefold and threshold current density decreased above 50%. High characteristic temperature and high beam quality were realized. © 2018 The Japan Society of Applied Physics

High-power, high-efficiency diode lasers emitting at 2 μm atmospheric transmission windows are required for applications such as gas or liquid sensing,[1,2] tunable diode laser absorption spectroscopy (TDLAS),[3,4] light detection and ranging (LiDAR),[5,6] direct optical communication,[7] and medical treatments.[8] In recent years, GaSb-based type-I quantum well (QW) diode lasers under continuous wave (CW) operation at room temperature (RT) in the spectral range from 1.9 to 3.5 μm have been demonstrated,[9,10] and optimal epitaxy structures have been used to improve the efficiency, threshold current (I_{th}), and vertical far-field (FF) performance of diode lasers, such as narrow symmetric waveguide design,[11] asymmetric waveguide design,[12] and cascade QW design.[13] The use of the broad-area (BA) waveguide is one of the most effective ways of realizing a high output power.[11] However, the BA waveguide leads to the operation of multiple lateral modes, and hence the beam quality is poor in the lateral direction.[14,15] In addition, the carrier diffusion in the BA waveguide will also result in the carrier leakage and accumulation at the ridge edges, deteriorating the FF performance.[16] Several approaches, such as nonuniform electrodes[16–18] and multiple microstripes,[19–21] were proposed to resolve these issues in GaAs-based BA lasers, but they also show some limitations including a large lateral divergence[19,20] and a sensitive double-lobed FF[19,21] owing to shallow and deep gain distribution modulations.

Given the intrinsic difference between III–As and III–Sb semiconductors,[22,23] such as the more lateral current spreading caused by the strong asymmetry conductivity between vertical and lateral directions resulting from the much higher hole mobility (750–1000 $cm^2 V^{-1} s^{-1}$ at 300 K)[22] of GaSb than of GaAs as a cap layer in the epitaxy structure, and the poor thermal conductivity of the III–Sb semiconductors,[23,24] the effectiveness of a BA waveguide with an etched microstripe structure in improving the carrier leakage, accumulation, and thermal behavior of GaSb-based BA lasers was demonstrated. The significantly improved threshold characteristics, output power, quantum efficiency, and single-lobed FF of GaSb-based BA lasers were demonstrated. The temperature-dependent light–current–voltage (*L–I–V*) curves and near-field (NF) and FF performance characteristics were measured and analyzed to clarify the mechanism behind those improvements.

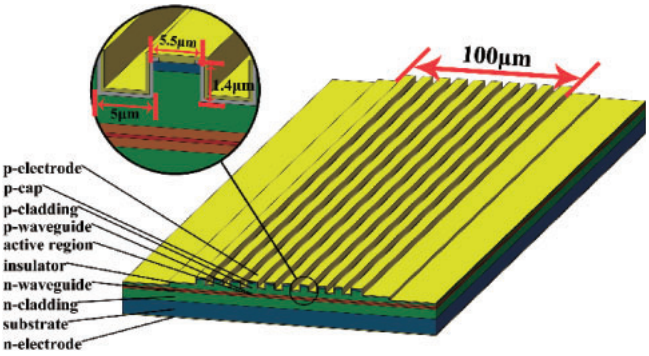

Fig. 1. Schematic diagram of GaSb-based QW MSBA lasers. The inset shows the structure in detail.

Figure 1 shows a schematic diagram of the proposed microstripe BA (MSBA) lasers. The MSBA laser consists of 10 microstripes of 5.5 μm width, and the distance between adjacent stripes is 5 μm. The total width of the BA waveguide is 100 μm and the depth of the microstripes is 1.4 μm, at which the top highly doped contact layer and part of the cladding layer are etched out. Hence, the microstripes form an alternative distribution of high-injection and low-injection areas. This can suppress the lateral spreading and leakage of carriers, which are mainly caused by the high plane conductivity and low vertical conductivity in diode lasers. The suppression of lateral current leakage will improve the injection efficiency and hence the energy conversion efficiency. The epitaxy structure was grown on a (100)-oriented 2-in. n^+-doped GaSb substrate using a solid-source VEECO Gen II molecular beam epitaxy (MBE) system. A 2-μm-thick n-doped ($\sim 5 \times 10^{17}$ cm^{-3}) $Al_{0.5}Ga_{0.5}As_{0.02}Sb_{0.98}$ cladding layer was grown after a 500-nm-thick buffer layer. A 10-nm-thick $In_{0.2}Ga_{0.8}Sb$ QW was sandwiched between the undoped top and bottom 270-nm-thick $Al_{0.2}Ga_{0.8}As_{0.02}Sb_{0.98}$ layers. Then, a 2-μm-thick p-doped ($\sim 1 \times 10^{18}$ cm^{-3}) $Al_{0.5}Ga_{0.5}As_{0.02}Sb_{0.98}$ cladding layer was added. A 250-nm-thick p^+-doped ($\sim 1 \times 10^{19}$ cm^{-3}) GaSb cap layer was grown on the top of the p-doped cladding layer for the Ohmic contact. The corresponding p- and n-type dopants were Be and Te, respectively.

To understand the role of the MSBA structure, theoretical simulations were performed. Figure 2 shows the distributions of current density in the QW of BA lasers at the injected

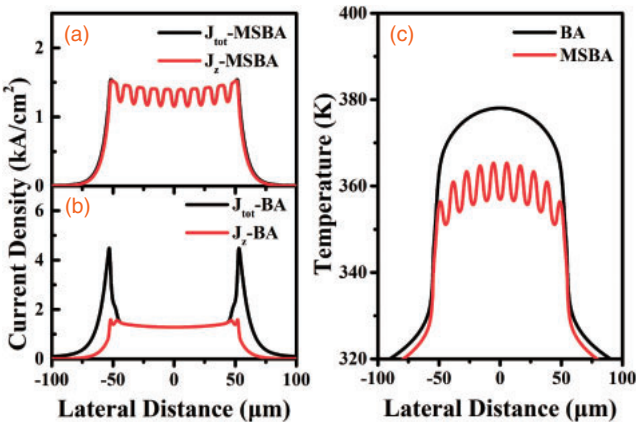

Fig. 2. Total current density along the lateral direction and current density distribution of (a) MSBA and (b) BA devices in QW with the injected current of 2.0 A. (c) Lateral temperature distribution in QW of MSBA and BA devices at thermal power density of 1.3×10^{16} W/m^3 with heat-sink temperature of 293 K.

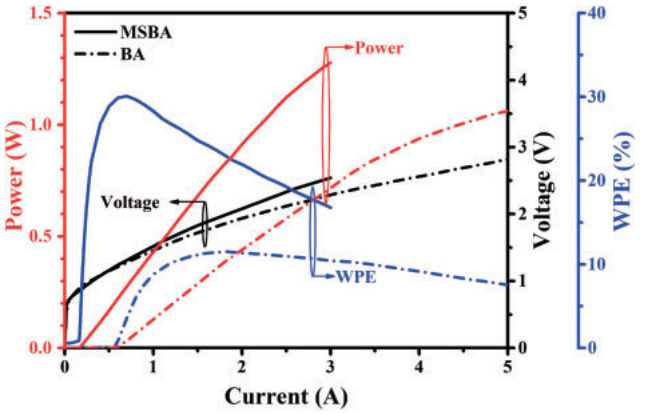

Fig. 3. CW *L–I–V* performance and WPE of MSBA and conventional BA lasers at 283 K.

currents of 2.0 A and 293 K along the lateral direction, which were calculated by COMSOL Multiphysics software. The parameters of carrier mobility and concentration were measured using Hall effects. The injected current density can be orthogonally decomposed into *x*- and *z*-axis components, and the current density along the *z*-axis component (J_z) was defined as the effective injected current density. The injection efficiency (η_{in}) can be expressed as the ratio of the integral of J_z to the total current density (J_{tot}). Figures 2(a) and 2(b) show the J_z and J_{tot} of MSBA and conventional BA lasers, respectively. It is evident that MSBA can reduce the lateral carrier leakage and accumulation at the edge of the BA waveguide, and hence improve η_{in}. The obtained η_{in} of the MSBA laser is as high as 97.8%; in contrast, that of the conventional GaSb-based BA laser is only 61.8%. Figure 2(c) shows the calculated temperature distribution in the MSBA and BA waveguides along the lateral direction. The thermal power density is 1.3×10^{16} W/m^3, corresponding to the total thermal power of 23.4 W. The heat-sink temperature is 293 K. The calculated temperature distribution for the MSBA laser shows a periodic fluctuation and a clear improvement owing to the periodic microstripes. The highest fluctuation is ~9 K, and the maximum improvement of temperature is above 22 K compared with those of the conventional BA lasers, which will contribute to the power improvement in devices.

The micron-scale stripes and etched interspace were defined by standard photolithography and inductively coupled plasma (ICP) dry etching. The structure was designed according to the distribution of the injected current and lateral modes. The etching depth was about 1.4 μm down to the p-doped cladding layer. After that, a mesa of 300 μm width and 1 μm depth was defined. Then, a 250-nm-thick Si_3N_4 insulation layer was deposited at 300 °C by plasma-enhanced chemical vapor deposition (PECVD). The contact window for a single microstripe was 3 μm wide and was etched by reactive ion etching (RIE). The contact metal was Ti–Pt–Au on the p-side. After the substrate thinning and polishing, n-type metal AuGeNi-Au was deposited. Finally, the wafer was cleaved into individual laser diodes with a cavity length of 1.5 mm. Laser chips were mounted on the copper heat sink by indium solder with the epi-side down and without facet coating for testing. BA devices with a ridge width of 100 μm were fabricated on the same wafer for comparison.

The measured *L–I–V* characteristics and wall-plug efficiencies (WPEs) of the InGaSb/AlGaAsSb QW BA devices (dash-dotted lines) and MSBA devices (solid lines) under the CW operation are shown in Fig. 3. The power was tested using a Thorlabs PM100 power meter with S148C integrating sphere photodiode power sensors. As shown in Fig. 3, MSBA presents a much lower threshold current and a significant improvement in efficiency, although the voltage increases. Obviously, the low threshold current can be attributed to the decreased injection area and improved threshold current density in MSBA lasers. The maximum WPE is more than doubled, which increases from 9.8 to 30.5% owing to the application of the microstripe structure. Moreover, the maximum slope efficiency increases from 0.298 to 0.544 W/A similarly to that mentioned above. The highest emission power of MSBA lasers from both facets is 1.28 W at 3 A, and the BA laser without microstripes can also realize an output power exceeding 1 W at 5 A. The MSBA structure also improves the property of heat dissipation. To confirm that, the thermal resistance (R_{th}) defined by $R_{th} = \Delta T/P_{heat}$ was estimated. Here, ΔT is the temperature difference between the heat source and the heat sink, and can be calculated from the dependence of wavelength on the operating temperature. P_{heat} is the heat power. The peak wavelength of the lasers under pulse operation (1 μs, 5 kHz) was measured and is plotted in Fig. 4(a) as a function of heat-sink temperature. The influence of self-heating can be ignored under the pulse operation, and the influence of temperature on the wavelength shift can be obtained, which is about 1.28 nm/K as shown in Fig. 4(a). The lasing spectra of BA and MSBA lasers at 288 K with the heat power of 1 W are shown in Figs. 4(b) and 4(c), respectively. The central wavelengths are respectively 1960.7 and 1966.9 nm for MSBA and BA lasers. Thus, the calculated R_{th} values are respectively 4.34 and 8.67 K/W for MSBA and BA lasers, corresponding to a significant decrease of 50%.

The temperature-dependent performance of BA lasers will reveal more functions of microstripes in the control of current leakage. Figure 5(a) shows the measured *L–I* characteristics of the InGaSb/AlGaAsSb QW BA lasers (dash-dotted lines) and MSBA lasers (solid lines) under CW operation from 283 to 303 K with a step of 5 K. Given the difference in the injection area for these two types of device, the current

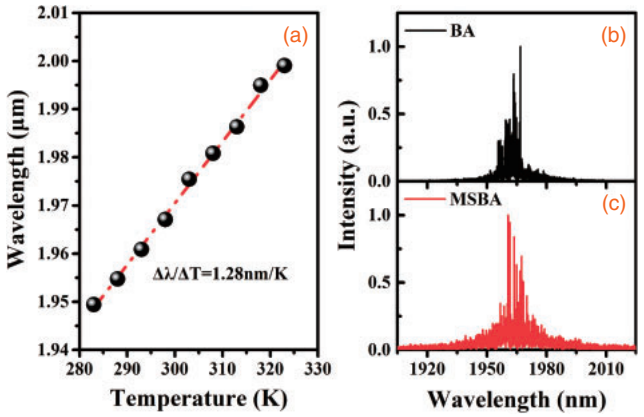

Fig. 4. (a) Lasing wavelength of MSBA laser as a function of operating temperature. (b) Lasing spectra of BA and MSBA lasers at 288 K with the heat power of 1 W.

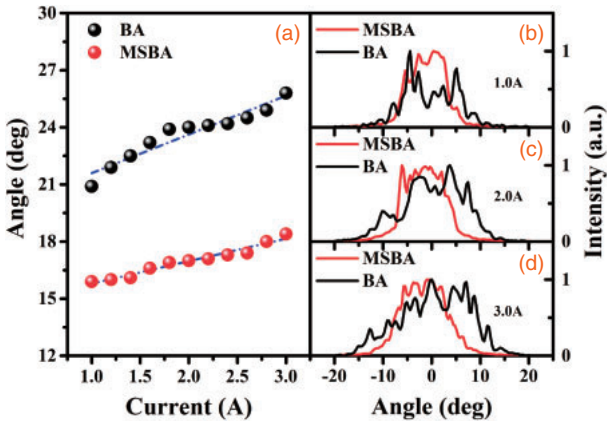

Fig. 6. (a) Lateral FF angles with 95% power content as a function of injected current. Panels (b), (c), and (d) are the corresponding lateral FF profiles at 1.0, 2.0, and 3.0 A, respectively.

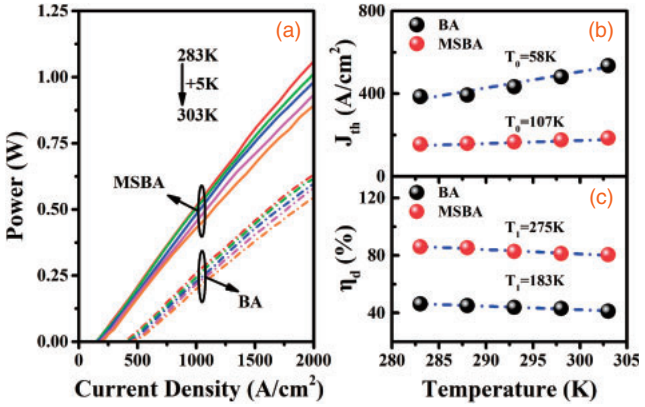

Fig. 5. (a) Temperature dependence of *L–I* characteristics from 283 to 303 K under CW operation. J_{th} (b) and η_d (c) of MSBA and BA devices as functions of temperature. The dash-dotted lines are the fitting results to the experimental data and the values of T_0 and T_1 are shown.

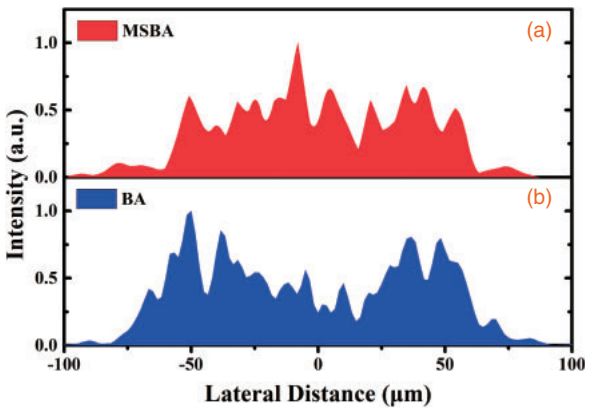

Fig. 7. Measured NF distributions of (a) MSBA and (b) BA lasers at injected current of 2 A.

density was selected as the horizontal axis in Fig. 5(a) for a more reasonable comparison. The threshold current density (J_{th}) of BA lasers is in the range of 345–478 A/cm^2 from 283 to 303 K; in contrast, the J_{th} of MSBA devices is in the range of 155–185 A/cm^2, corresponding to a significant decrease above 50%. The temperature-dependent J_{th} [$J_{th}(T) = J_0 \exp(T/T_0)$] shown in Fig. 5(b) presents characteristic temperature T_0 values of 107 K for MSBA lasers and 58 K for BA lasers. Figure 5(c) shows the temperature-dependent differential quantum efficiency (η_d) values of the lasers. By fitting the values by $\eta_d(T) = \eta_0 \exp(-T/T_1)$, the characteristic temperature T_1 values of differential quantum efficiency were obtained to be 275 and 183 K for MSBA and BA lasers, respectively. The evidently improved characteristic temperatures T_0 and T_1 for the MSBA structure can be explained as the suppressed carrier leakage and enhanced carrier injection efficiency, which are shown in Fig. 2.

The lateral divergences of the above devices under CW operation were measured using an Ophir Spiricon Pyrocam III beam profiling camera and are plotted in Fig. 6 as a function of injected current. The lateral FF angles were obtained with the definition of the 95% power content. As shown in Fig. 6, it was found that MSBA lasers have much lower lateral FF angles and a lower dependence on the injected current. The lateral FF angles of MSBA lasers increase from 15.9 to 18.4° with the injected current, corresponding to a widening of 2.5°. The lateral FF profiles of BA devices show more side lobes, and the lateral FF angles increase from 20.9 to 25.8° with the injected current. Thus, the FF angles of MSBA devices demonstrate an improvement of 30% compared with those of BA devices. The dependence of the lateral FF divergence on the injection decreases to 1.2°/A for MSBA devices; in contrast, it is 2.0°/A for BA devices. These results can be attributed to the suppressed lateral carrier accumulation (LCA) effects at the ridge edges, which were demonstrated to improve the injection dependence of the lateral FF.[16)]

To verify the results of the simulated lateral current distribution, the NF distributions were measured using the Ophir Spiricon Pyrocam III beam profiling camera with a 60× microscope objective. The NF characteristics of MSBA and BA lasers are shown in Figs. 7(a) and 7(b) for an injected current of 2 A, respectively. A comparative analysis of these NF profiles was performed. Figure 7 shows that the NF of the BA laser has more light at the edge of the device, which reveals more serious lateral current leakage and accumulation. This phenomenon agrees well with the results of the lateral current distribution calculated in Fig. 2, and this effect is one of the main reasons for FF blooming.

To estimate the beam quality of MSBA lasers, the beam waist radius is required, which can be obtained from the NF. Figure 8(a) shows the measured beam waist diameters of

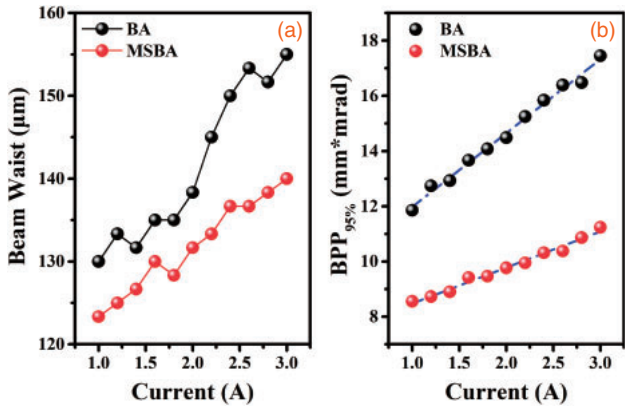

Fig. 8. (a) Beam waist diameter and (b) $BPP_{95\%}$ values of BA and MSBA lasers in lateral direction with 95% power content as functions of injected current.

MSBA and BA lasers as a function of injected current; such results are obtained from the definition of 95% power content of normalized NF intensity. The MSBA laser shows a much lower beam waist than the BA laser. As to the beam quality, it can be described by the beam parameter product (BPP) and written as $BPP_{95\%} = \omega_{95\%}\theta_{95\%}/4$. Here, $BPP_{95\%}$, $\omega_{95\%}$, and $\theta_{95\%}$ are the BPP, beam waist diameter, and FF divergence angle with 95% power content, respectively. Given that the MSBA structure affects mainly the beam quality in the lateral direction, the lateral $BPP_{95\%}$ was estimated and is shown in Fig. 8(b). The lateral BPPs of 8.6 and 11.2 mm × mrad are demonstrated by the MSBA laser at 1 and 3 A, corresponding to the improvements of 28 and 36% compared with those of the BA laser, respectively. The dependence of the lateral BPP on the injection decreases to 1.30 mm × mrad/A for the MSBA laser; in contrast, it is 2.67 mm × mrad/A for the BA laser. These results can be attributed to the narrow beam waist and low lateral FF divergence due to the suppressed LCA at the ridge edges[16] by microstripes.

In summary, we demonstrated high-power, high-efficiency GaSb-based diode lasers with the MSBA structure. It was shown that the MSBA structure could significantly improve the current injection efficiency and hence reduce the carrier leakage and accumulation at the ridge edges. The energy conversion efficiency of the MSBA structure was more than threefold that of the conventional BA structure. The characteristic temperatures of threshold and quantum efficiency were respectively increased to 107 and 275 K. A more stable and higher beam quality was realized. We believe that these results will contribute to the development of high-power and high-beam-quality GaSb-based diode devices.

Acknowledgments This work was supported by the National Natural Science Foundation of China (Nos. 61404138, 61474119, 61435012, and 61774756), the National Basic Research Program of China (2014CB643903), the International Science Technology Cooperation Program of the Chinese Academy of Sciences (No. 181722KYSB20160005), Jilin Provincial Natural Science Foundation (Nos. 20160101243JC, 20160520095JH, and 20150520105JH), and the Opened Fund of the State Key Laboratory on Integrated Optoelectronics (No. IOSKL2016KF15).

1) Q. Gaimard, M. Triki, T. Nguyen-Ba, L. Cerutti, G. Boissier, R. Teissier, A. Baranov, Y. Rouillard, and A. Vicet, Opt. Express **23**, 19118 (2015).
2) W. W. Bewley, C. L. Felix, I. Vurgaftman, E. H. Aifer, L. J. Olafsen, J. R. Meyer, L. Goldberg, and D. H. Chow, Appl. Opt. **38**, 1502 (1999).
3) L. Dong, F. K. Tittel, C. Li, N. P. Sanchez, H. Wu, C. Zheng, Y. Yu, A. Sampaolo, and R. J. Griffin, Opt. Express **24**, A528 (2016).
4) A. Salhi, D. Barat, D. Romanini, Y. Rouillard, A. Ouvrard, R. Werner, J. Seufert, J. Koeth, A. Vicet, and A. Garnache, Appl. Opt. **45**, 4957 (2006).
5) S. Forouhar, R. M. Briggs, C. Frez, K. J. Franz, and A. Ksendzov, Appl. Phys. Lett. **100**, 031107 (2012).
6) E. Dale, M. Bagheri, A. B. Matsko, C. Frez, W. Liang, S. Forouhar, and L. Maleki, Opt. Lett. **41**, 5559 (2016).
7) N. S. Prasad, in *Free-Space Laser Communications: Principles and Advances*, ed. A. K. Majumdar and J. C. Ricklin (Springer, New York, 2008) Chap. 8.
8) R. W. Waynant, I. K. Ilev, and I. Gannot, Philos. Trans. Roy. Soc. London, Ser. A **359**, 635 (2001).
9) L. Shterengas, G. Kipshidze, T. Hosoda, R. Liang, T. Feng, M. Wang, A. Stein, and G. Belenky, IEEE J. Sel. Top. Quantum Electron. **23**, 1 (2017).
10) G. Belenky, L. Shterengas, M. V. Kisin, and T. Hosoda, in *Semiconductor Lasers*, ed. A. Baranov and E. Tournie (Woodhead Publishing, Cambridge, U.K., 2013) p. 441.
11) M. Rattunde, J. Schmitz, G. Kaufel, M. Kelemen, J. Weber, and J. Wagner, Appl. Phys. Lett. **88**, 081115 (2006).
12) J. Chen, G. Kipshidze, and L. Shterengas, IEEE J. Quantum Electron. **46**, 1464 (2010).
13) T. Hosoda, T. Feng, L. Shterengas, G. Kipshidze, and G. Belenky, Appl. Phys. Lett. **108**, 131109 (2016).
14) A. I. Bawamia, B. Eppich, K. Paschke, H. Wenzel, F. Schnieder, G. Erbert, and G. Tränkle, Appl. Phys. B **97**, 95 (2009).
15) P. Crump, S. Böldicke, C. M. Schultz, H. Ekhteraei, H. Wenzel, and G. Erbert, Semicond. Sci. Technol. **27**, 045001 (2012).
16) C. Lindsey, P. Derry, and A. Yariv, Electron. Lett. **21**, 671 (1985).
17) B. Bo, X. Gao, L. Wang, H. Li, and Y. Qu, IEEE Photonics Technol. Lett. **16**, 1248 (2004).
18) P. Salet, F. Gerard, T. Fillion, A. Pinquier, J. L. Gentner, S. Delepine, and P. Doussiere, IEEE Photonics Technol. Lett. **10**, 1706 (1998).
19) G. Sobczak, E. Dąbrowska, M. Teodorczyk, K. Krzyżak, and A. Malag, IEEE J. Quantum Electron. **50**, 890 (2014).
20) M. V. Maximov, Y. M. Shernyakov, I. I. Novikov, L. Y. Karachinsky, N. Y. Gordeev, U. Ben-Ami, D. Bortman-Arbiv, A. Sharon, V. A. Shchukin, N. N. Ledentsov, T. Kettler, K. Posilovic, and D. Bimberg, IEEE J. Sel. Top. Quantum Electron. **14**, 1113 (2008).
21) R. Platz, G. Erbert, W. Pittroff, M. Malchus, K. Vogel, and G. Tränkle, High Power Laser Sci. Eng. **1**, 60 (2013).
22) J. Piprek, *Semiconductor Optoelectronic Devices* (Academic Press, Boston, MA, 2003) Chap. 3.
23) J. Piprek, *Semiconductor Optoelectronic Devices* (Academic Press, Boston, MA, 2003) Chap. 6.
24) L. Piskorski and R. P. Sarzala, Opt. Appl. **46**, 227 (2016).